PROCEEDINGS OF SPIE

SPIEDigitalLibrary.org/conference-proceedings-of-spie

Shape-adjustable heliostats: designs for individuals and fields for > 3000 concentration

N. Didato, R. Angel, M. Rademacher

N. Didato, R. Angel, M. Rademacher, "Shape-adjustable heliostats: designs for individuals and fields for > 3000 concentration," Proc. SPIE 12671, Advances in Solar Energy: Heliostat Systems Design, Implementation, and Operation, 126710D (4 October 2023); doi: 10.1117/12.2681483

SPIE.

Event: SPIE Optical Engineering + Applications, 2023, San Diego, California, United States

Shape-adjustable heliostats – designs for individuals and fields for > 3000 concentration

N. Didato*[a], R. Angel[a], M. Rademacher[a]
[a]Department of Astronomy and Steward Observatory, University of Arizona, 933 N. Cherry Ave., Tucson, AZ, USA 85721

ABSTRACT

Shape-adjustable heliostats can maintain a focused image of the solar disc on a receiver target throughout the day, as the angle of incidence (AOI) changes on the reflector. This requires the heliostat reflector to be deformed into a unique biconic concave shape dependent on AOI. The reflector comprises a single rectangular sheet of silvered float glass mounted to a steel frame. Its shape is set initially, by adjusting the height of mounting points, to the biconic shape required for imaging at 60 degrees AOI. Shapes for other AOIs are obtained by twisting the frame from its four corners and center. A finite element model was made of a heliostat designed to form a disc image on a 130 m distant receiver using a single sheet glass reflector, 1/8" thick x 130" x 96", supported by 58 points on a rectangular tube frame structure weighing 120 kg. Analysis shows an overall RMS slope error <1 mrad for all AOI from 0 to 70 degrees. Without twisting, the RMS slope error would be ~3.5 mrad at 0° and 70° AOI. Preliminary results from analysis of slope error maps generated from the FE model indicate encircled energies within the ideal solar disc radius of >85% are achievable. Models of fields of closely packed heliostats of this type, on target axis mounts, demonstrate a geometrical throughput into the receiver of >73% of the total mirror area, after accounting for blocking, shadowing, and cosine loss. In one model, with 450 heliostats powering five compound parabolic concentrators at a receiver, a concentration of > 3,000 was obtained at powers > 1 MW, through much of the day.

Keywords: Heliostat, Adjustable, Twisting, Angle of incidence, Focus, Encircled energy, Slope error

1. INTRODUCTION

To increase electrical generation efficiency, and to increase thermal processing capabilities, heliostat receivers need to achieve temperatures beyond what is currently achievable, and thus higher concentrations of sunlight are required. One way to increase concentration is by using flat heliostats to direct sunlight onto a large static concave paraboloidal reflector to focus sunlight onto the receiver target. Various CSP systems use this method, but for heliostat fields focusing directly to a receiver, the angle of incidence (AOI) on any reflector changes as the sun moves across the sky throughout the day. To maintain a focus on the receiver under these circumstances, the reflector shape must also change. The shape required for focusing sunlight striking at different AOIs are different concave biconics, whose two principal radii of curvature in the tangential and sagittal directions are functions of the AOI and must be rotated to be in line with and perpendicular to the plane of incidence respectively.

One concept for an actively shaped heliostat is described by Angel et al. [1]. In this embodiment, a hexagonal reflector was used on an alt-az mount, and the biconic curvatures were adjusted using 3 pairs of actuators pushing and/or pulling on the 6 corners of the reflector frame. A disadvantage of using an alt-az mount is that the orientation of the plane of incidence is constantly changing with respect to the reflector, as well as the two biconic radii of curvature, and shape adjustment requires computer control of three degrees of freedom.

The more recent concept described in Angel et al. [2] employs a rectangular reflector on a target-axis mounted system, with only mechanical coupling needed to control its shape through the day. This is made possible because the target axis of the dual axis mount points directly to the receiver, and thus lies in the plane of incidence. To move the image of the sun onto the target, the target axis is rotated until the second axis denoted as the "cross-axis", which is perpendicular to the target axis, is set also perpendicular to the plane of incidence. Rotation of the cross axis then is used to set the correct AOI. In this way, the plane of incidence is fixed in orientation with respect to the heliostat reflector. Figure 1 shows the shape of the glass rectangle with the two principal curvatures at 45 degrees to the rectangle edges. The desired different biconic

Advances in Solar Energy: Heliostat Systems Design, Implementation, and Operation, edited by Guangdong Zhu, Marc Röger, Zhifeng Wang, Proc. of SPIE Vol. 12671, 126710D · © 2023 SPIE · 0277-786X · doi: 10.1117/12.2681483

shapes are adjusted by twisting the glass from its 4 corners and center, as described by Rademacher et al, [3]. The reflector is attached to the cross-axis drive at 45°, so that the tangential axis is oriented perpendicular to the cross-axis, and the required biconic shapes are attained using a mechanical linkage with two mechanical cam couplings to the cross-axis drive.

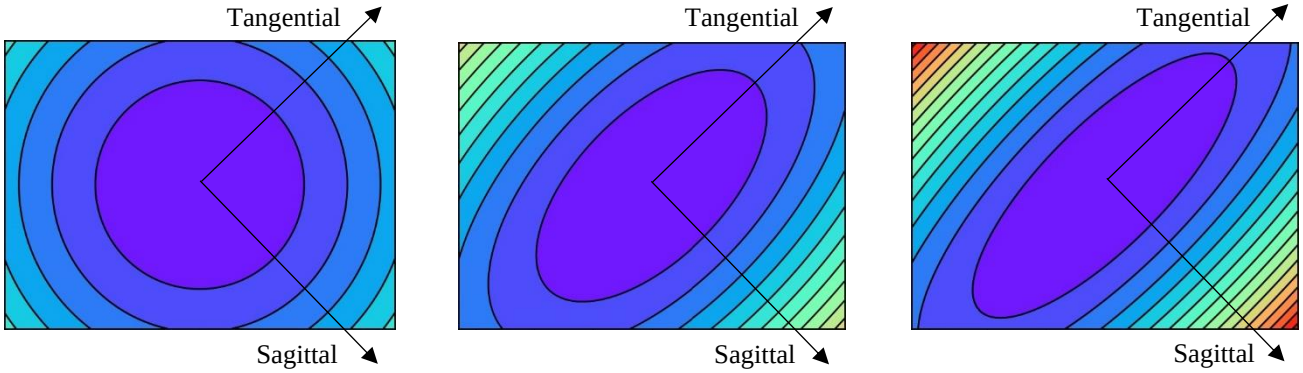

Figure 1. Complete biconic shapes for 0 (left), 60 (middle), and 70 (right) degrees angle of incidence. Tangential and sagittal axes are shown.

*ndidato@arizona.edu

2. HELIOSTAT DESIGN

2.1 Required biconic reflector shapes for a target-axis mounted heliostat

The required biconic for a reflector surface to focus sunlight on a receiver target using a target-axis mount is function of the angle of incidence (AOI). The ideal radii of curvature of the biconic, in the tangential plane (R_T) and sagittal plane (R_S), are given by:

$$R_T = \frac{R}{\cos(AOI)} \tag{1}$$

$$R_s = Rcos(AOI) \tag{2}$$

where AOI is the angle of incidence and R is the radius of curvature, which is equal to twice the distance between the heliostat and the receiver (i.e., focal length).

Another way to express the required biconic shapes is by orthogonal optical polynomials. Generally, a biconic is a superposition of three orthogonal polynomials: Power, oblique astigmatism, and vertical astigmatism. The superposition of the two astigmatism modes is used ensure proper orientation of the tangential plane with the plane of incidence. For a target-axis system, this orientation is done with the target axis drive, so only the oblique astigmatism mode is required.

The overall biconic shape is given by equations 3-5:

$$a_1 = \frac{1}{4}\left(\frac{1}{R_T} + \frac{1}{R_s}\right) \tag{3}$$

$$a_2 = \frac{1}{4}\left(\frac{1}{R_T} - \frac{1}{R_s}\right) \tag{4}$$

$$Z(x,y) = a_1(x^2 + y^2) + a_2(2xy) \tag{5}$$

where a_1 and a_2 are the optical coefficients for the power and oblique astigmatism modes, which are functions of the tangential and sagittal radii of curvature.

2.2 Heliostat frame design

The reflector is a single 96 x 130 in. rectangular sheet of 1/8 in. thick, silvered float glass mounted to a flat steel frame. The glass is attached to the steel frame on 58 points with a silicone adhesive. Attached to the rear side of the frame is a central mast which connects the frame to the post, along with two pairs of back struts which connect the corners of the frame to the shape-changing mechanism on the cross-axis drive. The frame layout is shown in Figure 2.

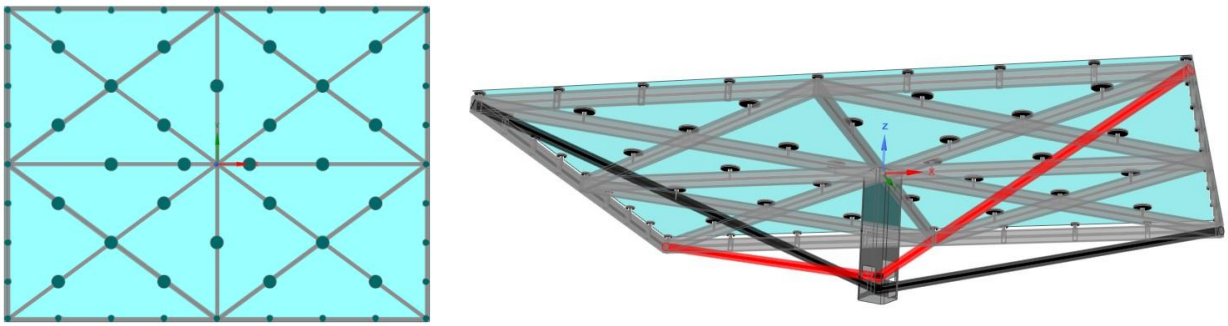

Figure 2. Heliostat reflector frame design top-down (left) and side view showing the back struts and central mast (right).

Since the biconc is symmetrical about the origin, the displacement of opposite corners will be equal for every required shape, thus they can be actuated in pairs as shown in Figure 2.

The steel frame is comprised 1/16 in. wall, 3x1 in. rectangular tubes with the long dimension oriented perpendicular to the glass. The back struts are 2 in. diameter tubes with a 1/8 in. wall. The central mast is a 6x6 in, square tube with a ¼ in. wall.

To reduce the amount of force required to bend the frame into the proper shape, the 58 points are initially adjusted in height to induce a "neutral biconic", which is in the middle of the corner-corner sag range from 0 degrees AOI to 70 degrees AOI. This neutral shape was determined to be the required biconic at 60 degrees AOI.

3. EVALUATION OF HELIOSTAT PERFORMANCE

3.1 Finite element model

A finite element model of the heliostat reflector and frame was created to analyze the quality of the induce shape changes. This includes bending accuracy, gravity loads, and a nominal operating wind load. Gravity and wind were evaluated for a heliostat at an elevation angle of 60 degrees, which was determined to be the worst case for combined gravity and wind loading using methods described in Peterka 1992 [4]. An 11-mph headwind was used as the nominal wind speed and direction, which was chosen based on the wind speed distribution measured at Lee Ranch in 2003 [5]. A focal length of 130 m was chosen for this analysis, which was selected to represent the outermost row of a heliostat field, whose solar image will be more sensitive to shape distortions than the innermost rows with shorter focal lengths.

The model is comprised of mostly shell (mirror and central mast) and beam elements (frame and back struts). The mirror is connected to the frame by beam elements representing ¼ - 20 bolts, with a solid pad and silicone adhesive bond between the bolts and the mirror. The FE model contains roughly 130,000 nodes and is shown in Figure 3.

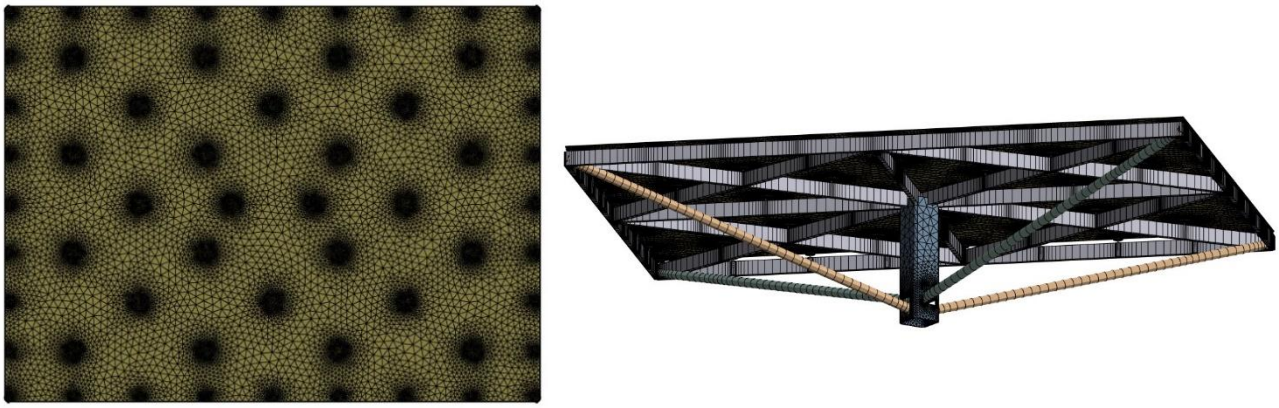

Figure 3. Finite element model of the mirror (left) and mirror + frame (right)

The overall goal of the FE analysis was to determine the slope error of the reflector relative to the ideal biconic. The slope maps were then post-processed to calculate the encircled energy within the radius of a perfect solar image on the receiver.

Non-linear deformation behavior was used to capture the effect of hoop stresses, which are developed when a flat surface is bent in both principal directions.

3.2 Encircled energy calculation

Encircled energy is defined here as the ratio of focused energy contained within the diameter of a perfect solar image to the total energy. This is calculated from the slope maps produced by the FE model in 5 steps:

1. Slope maps are converted into kernel density estimation (KDE) plots in both the x and y directions.
2. A point spread function (PSF) is created by multiplying the x and y KDEs together.
3. An ideal solar disc is created on a 100x100 grid in units of normalized intensity, accounting for solar limb darkening.
4. The PSF is overlayed on each point of the solar disc and summed to generate the solar image in normalized intensity.
5. Normalized intensity is integrated, and encircled energy is calculated as the ratio of intensity inside a 4.62 mrad radius (angular radius of the sun) to the total intensity from positive to negative infinity.

Encircled energy was calculated assuming perfect pointing, and with a 0.5 mrad pointing error from tracker flexure during wind gusts. RMS slope errors and encircled energy at different angles of incidence are summarized in Figure 4.

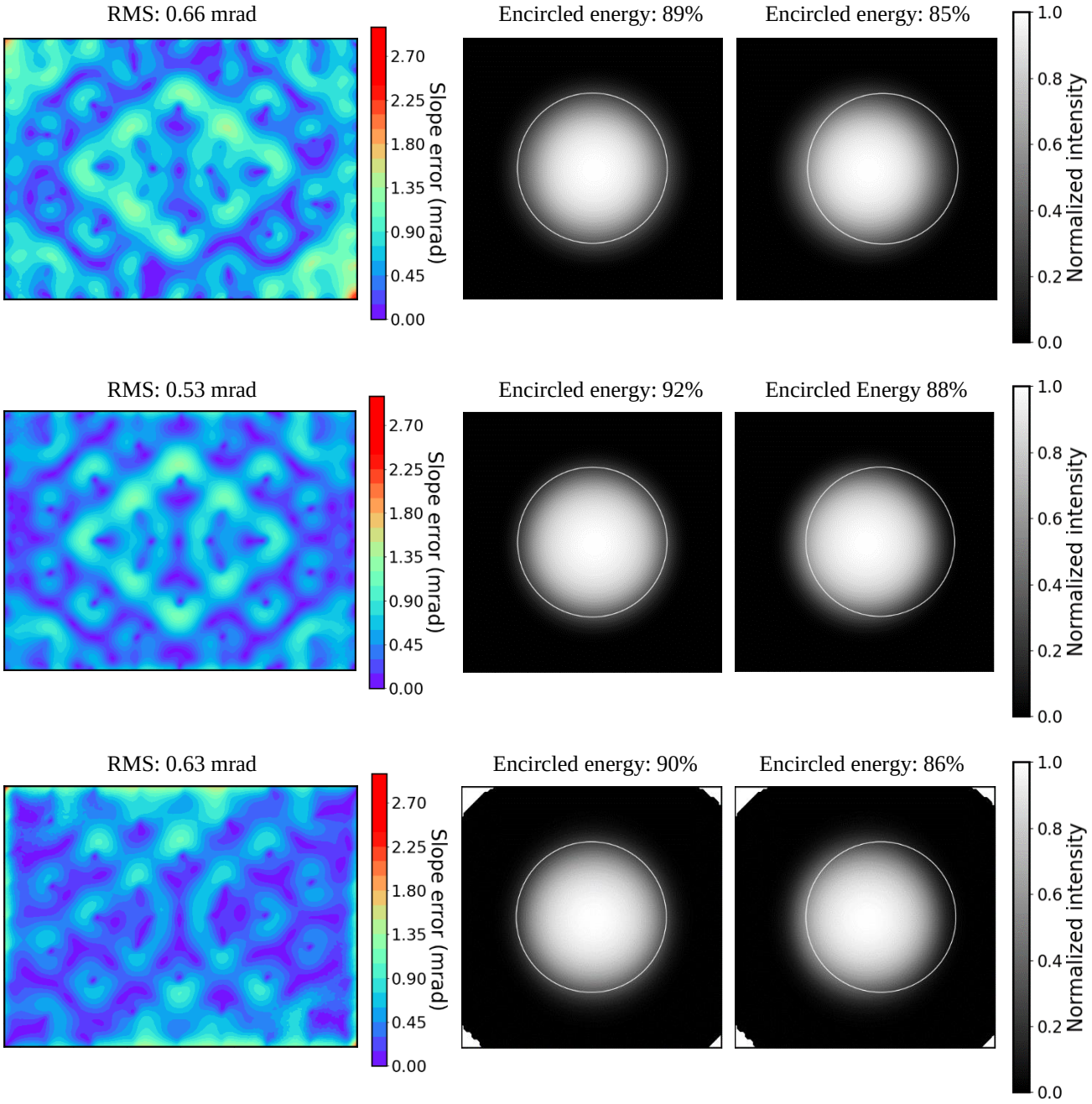

Figure 4. Slope error maps calculated from FE model (left) and encircled energy with perfect pointing (middle) and a 0.5 mrad pointing error (right) for AOIs of 0 degrees (top), 60 degrees (middle), and 70 degrees (bottom).

With an 11-mph average headwind and gravity load at the worst-case elevation angle of 60 degrees, the mirror RMS slope error is less than 0.7 mrad, and mis-pointing is less than 0.5 mrad. The combined effect of these errors yields and encircled energy of greater than 85% relative to a perfect solar image.

4. HELIOSTAT FIELD DESIGN

4.1 CPC reactor field design

A heliostat field was designed to focus light into compound paraboloidal concentrators (CPCs). The field consists of 5 groups of 89 heliostats ranging from 70-110 m in focal length, which each group focusing light into a conical CPC with a 1 m diameter entrance pupil and 23-degree cone angle as described in Brendelberger et al. [6]. Since the solar disc subtends a 0.5-degree angle in the sky, the maximum possible focal length that can be used to focus sunlight into a 1 m aperture is 110 m. A schematic of a CPC is shown in Figure 5.

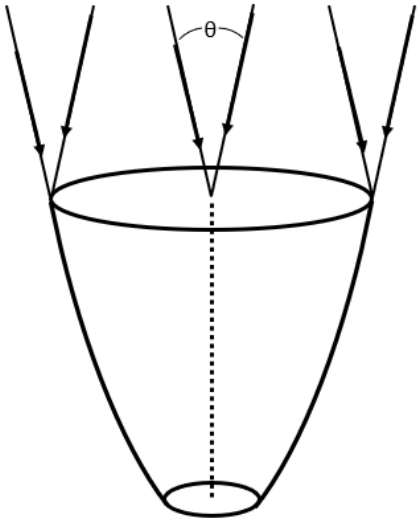

Figure 5. Schematic of a CPC receiver showing the incident rays and cone angle.

4.2 Field model

A Python-based field model was created to aid with the design of the heliostat field. The purpose of this model was to determine the optimal receiver height, receiver pointing angle, heliostat focal length range, and heliostat packing density to maximize the receiver throughput. This was achieved in 5 steps:

1. Trace the 23-degree cone angle from the receiver location to the ground. This projects an ellipse on the ground of which all heliostats must be within.
2. Determine the receiver height and pointing angle that creates the largest ellipse on the ground without exceeding a slant distance of 110 m.
3. Fit as many heliostats into this truncated ellipse as possible such that they don't contact one another at any pointing angle.
4. Plot the rectangular heliostats from the view of the receiver and the sun to evaluate shadowing and blocking losses.
5. Adjust heliostat spacing to minimize shadowing/blocking without removing too many from the ellipse to maximize effective heliostat area.

The field layout was generated using a similar algorithm presented in Collado et al. [7] and optimized in the receiver view by adjusting the spacing parameters. To view the heliostat field in the receiver view, a series of coordinate transformations are performed. First, the 4 corners of the reflector are plotted in the mirror coordinate system, which the sagittal and

tangential axes shown in Figure 1 serve as the x and y axes respectively. The 4 corner coordinates are then transformed into the global coordinate system, where x and y and the east-west and north-south directions respectively, and z is altitude.

When pointed correctly, the heliostat normal vector will be pointed between the target-axis vector and the solar vector. The unit normal vector of the nth heliostat is given by:

$$\boldsymbol{n}_n = \frac{\boldsymbol{t}_n + \boldsymbol{s}}{\|\boldsymbol{t}_n + \boldsymbol{s}\|} \tag{6}$$

where $\mathbf{t}_n$ is the unit vector pointing from the nth heliostat to the receiver, $\mathbf{s}$ is the unit vector pointing to the sun, and the brackets denote the vector norm. The sagittal and tangential axes in the global coordinate system are then given by:

$$\boldsymbol{sag}_n = \frac{\boldsymbol{t}_n \times \boldsymbol{n}_n}{\|\boldsymbol{t}_n \times \boldsymbol{n}_n\|} \tag{7}$$

$$\boldsymbol{tan}_n = \frac{\boldsymbol{n}_n \times \boldsymbol{sag}_n}{\|\boldsymbol{n}_n \times \boldsymbol{sag}_n\|} \tag{8}$$

where × denotes the cross-product. The coordinates of the 4 corners (k = 1 to 4) of the heliostat reflector are then given in the global coordinate system by:

$$x_{n,k} = h_{x,n} + g_{x,k} sag_{x,n} + g_{y,k} tan_{x,n} \tag{9}$$

$$y_{n,k} = h_{y,n} + g_{x,k} sag_{y,n} + g_{y,k} tan_{y,n} \tag{10}$$

$$z_{n,k} = g_{x,k} sag_{z,n} + g_{y,k} tan_{z,n} \tag{11}$$

where $h_{x,n}$ and $h_{y,n}$ are the x and y coordinates of the nth heliostat in the field, $g_{x,k}$ and $g_{y,k}$ are the x and y coordinates of the kth corner in the mirror coordinate system, and $sag_{x,n}$, $tan_{x,n}$, $sag_{y,n}$, and $tan_{y,n}$ are the x and y components of the $\mathbf{sag}_n$ and $\mathbf{tan}_n$ vectors. The components of the vectors that point from the receiver to the 4 corners of the nth reflector in the global coordinate system are given by:

$$v_{x,n,k} = x_{n,k} \tag{12}$$

$$v_{y,n,k} = y_{n,k} \tag{13}$$

$$v_{z,n,k} = z_{n,k} - r \tag{14}$$

where r is the receiver height. The +z direction in the receiver coordinate system, denoted $\mathbf{z}_{rec}$, is defined as the principal axis of the receiver's cone, pointing toward the ground. The receiver system x and y axes, denoted $\mathbf{x}_{rec}$ and $\mathbf{y}_{rec}$, are defined as:

$$\boldsymbol{x}_{rec} = \frac{\boldsymbol{z}_{rec} \times \boldsymbol{zen}}{\|\boldsymbol{z}_{rec} \times \boldsymbol{zen}\|} \tag{15}$$

$$\boldsymbol{y}_{rec} = \frac{\boldsymbol{z}_{rec} \times \boldsymbol{x}_{rec}}{\|\boldsymbol{z}_{rec} \times \boldsymbol{x}_{rec}\|} \tag{16}$$

where **zen** is the zenith direction. The receiver to mirror corners vector components in the receiver coordinate system are given by:

$$v'_{x,n,k} = \hat{\boldsymbol{v}}_{n,k} \cdot \boldsymbol{x}_{rec} \tag{17}$$

$$v'_{y,n,k} = \hat{\boldsymbol{v}}_{n,k} \cdot \boldsymbol{y}_{rec} \tag{18}$$

$$v'_{z,n,k} = \hat{\boldsymbol{v}}_{n,k} \cdot \boldsymbol{z}_{rec} \tag{19}$$

where $\mathbf{v}_{n,k}$ is the unit vector pointing from the receiver to the kth corner in the global coordinate system and · denotes the dot product. The receiver view of the heliostat field is then a plot of $v'_{x,n,k}$ vs $v'_{y,n,k}$ in units of radians or degrees. A similar approach is taken to plot the heliostat field from the viewpoint of the sun, except the vectors from the receiver to the corners of the reflectors are not normalized. This gives and orthographic view from the sun instead of a perspective view.

4.3 Optimized field

The optimal receiver position was determined to be 40 m high, pointing downward at a 30-degree angle relative to the horizon. The optimized field layout for a single CPC receiver is shown in Figures 6 and 7.

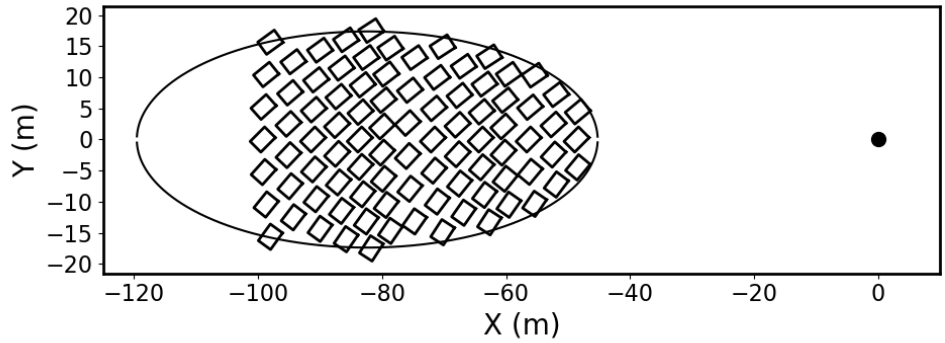

Figure 6. Plan view of a single field of 89 heliostats. The inner row is spaced 45 m from the receiver tower, and the outer row extends out to 100 m from the tower.

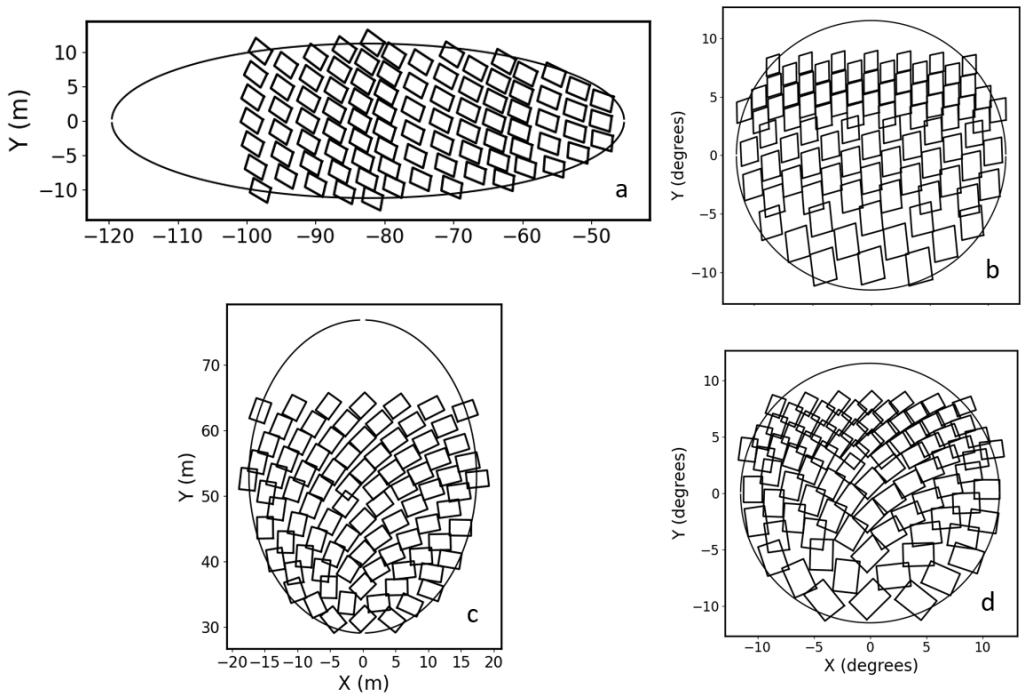

Figure 7. Field of 89 heliostats as viewed from the sun (a) (c) and the receiver (b) (d) for a solar elevation of 40 degrees, and solar azimuth positions of 90 degrees (a) (b) and 180 degrees (c) (d).

The complete heliostat field will consist of 5 groups of the above layout, with a total of 445 heliostats. A schematic of the complete field is shown in Figure 8.

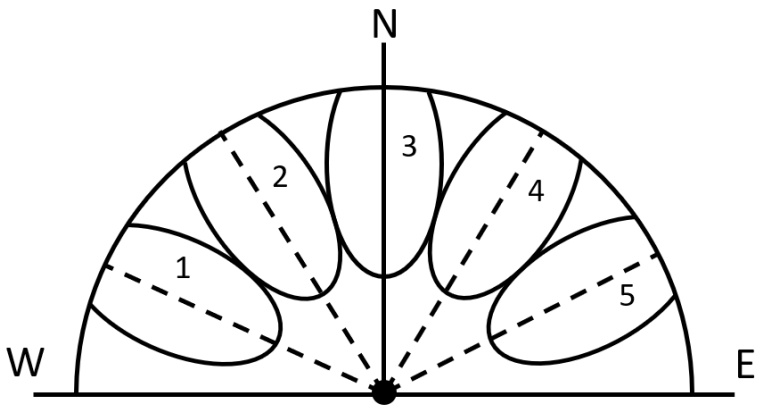

Figure 8. Group of 5 heliostat fields, each focusing sunlight on a CPC receiver mounted on the central tower.

4.4 Geometric throughput calculation

The total geometric throughput is a function of 3 things: shadowing by adjacent heliostats (shadowing), blocking of reflected light by anterior rows of heliostats (blocking), and reduction of projected mirror area proportional to the cosine of the angle of incidence (cosine loss). The angle of incidence for various solar positions corresponding to different times of the day were extracted from the field model, and cosine loss for each solar position was computed. The sun and receiver views for various solar positions corresponding to different times of day were used to estimate the shadowing and blocking loss fraction over the course of a day. The effective mirror area is given by:

$$A_{eff} = A_{total}(1 - f_{sh})(1 - f_{bl})(f_{cos}) \tag{20}$$

where f_{sh} is the shadowing fraction, f_{bl} is the blocking fraction, f_{cos} is the average cosine factor, and A_{total} is the total mirror area. Each mirror has an area of 8 m^2, giving a total field mirror area of 3560 m^2. The effective mirror area at different times of day for each CPC is shown in Table 1.

Table 1. Effective mirror area of a field powering 5 CPCs at different times of day on the equinox.

	CPC 1	**CPC 2**	**CPC 3**	**CPC 4**	**CPC 5**	**Total**
Time	**Effective mirror area (m^2)**					
6	0	0	0	0	0	0
7	420	361	346	331	288	1747
8	594	554	526	490	430	2593
9	596	617	615	564	480	2872
10	572	586	632	606	521	2916
11	613	578	609	628	578	3005
12	624	621	599	621	624	3089
1	578	628	609	578	613	3005
2	521	606	632	586	572	2916
3	480	564	615	617	596	2872
4	430	490	526	554	594	2593
5	288	331	346	361	420	1747
6	0	0	0	0	0	0

Taking the 8 am and 4 pm effective areas to be the average over the day, the geometric throughput relative to the total field mirror area is 73%.

5. TOTAL OPTICAL THROUGHPUT CALCULATION

Now that encircled energy and geometric throughput have characterized, the total optical throughput can be estimated with a few additional assumptions about the optical surfaces involved in the system. The heliostat reflectivity, CPC reflectivity, and CPC vacuum window transmission are all assumed to be 90%. The total optical throughput is calculated and shown in Table 2.

Table 2. Total optical throughput summary

Throughput source	Fraction
Encircled energy	0.85
Geometric throughput	0.73
Heliostat reflectivity	0.9
CPC reflectivity	0.9
CPC window transmission	0.9
Solar concentration calculation	
Total throughput (fraction of heliostat area)	0.45
Total heliostat area	3560 m^2
Effective area of sunlight	1602 m^2
Total CPC pupil area	3.93 m^2
CPC concentration	10x
Total solar concentration	**4076x**

One thing to note is the encircled energy was computed relative to a perfect solar image at a 130 m focal length. The CPC aperture is sized for a perfect solar image at 110 m focal length, which will likely have a similar encircled energy fraction, but the shorter focal length heliostats in the field will be able to form smaller solar images, giving more margin for blurring and mis-pointing. The calculated value of 4076 suns is therefore a lower limit to the total concentration achievable by this field.

6. CONCLUSIONS

For a 130 m focal length heliostat, subject to an 11-mph headwind in the worst-case pointing condition, the RMS slope error under is 0.7 mrad and the tracker mis-pointing is under 0.5 mrad. This yields an encircled energy of greater than 85% relative to a perfect solar image with perfect tracking. The geometric throughput of 5 groups of 89 heliostats, each focusing light onto a CPC receiver, is estimated to be 73% on average throughout the course of a day. The total solar concentration in the reaction chamber of the CPC is greater than 4000 suns. For a direct normal irradiance (DNI) of 1000 W/m^2, the entire field is expected to generate > 4 MW of heat at the receivers.

REFERENCES

[1] R. Angel, R. Eads, N. Didato, N. Emerson, C. Davila, “Actively Shaped Focusing Heliostat,” AIP Conference Proceedings Vol. 2445 (2022).

[2] R. Angel, M. Rademacher, N. Didato, “Heliostat with Automatic Shape Adjustment for High Concentration Throughout the Day”, SolarPACES (2022)

[3] M. Rademacher, R. Angel, N. Didato, “Shape-adjusting mechanism for a heliostat reflector on a target-oriented mount”, SPIE (2023)

[4] J. A. Peterka, R. G. Derickson, “Wind Load Design Methods for Ground-Based Heliostats and Parabolic Dish Collectors,” Sandia National Laboratories, SAND92-7009 (1992).

[5] Global Energy Concepts., “Sandia National Laboratories New Mexico Wind Resource Assessment Lee Ranch,” February 2003

[5] S. Brendelberger et al., “Study of a new receiver-reactor cavity system with multiple mobile redox units for solar thermochemical water splitting,” Solar Energy 235, pp. 118-128 (2022)

[6] F. J. Collado, J. Guallar, “Quick design of regular heliostat fields for commercial solar tower power plants,” Energy 178, pp. 115-125 (2019)